MDPI

Article

Evaluation of the Performance of Commercial High Temperature Superconducting Tapes for Dynamo Flux Pump Applications

Giacomo Russo and Antonio Morandi *

Department of Electrical, Electronic and Information Engineering, University of Bologna, 40126 Bologna, Italy; giacomo.russo5@unibo.it
* Correspondence: antonio.morandi@unibo.it

Abstract: High Temperature Superconducting (HTS) dynamo flux pumps are a promising alternative to metal current leads for energization and the persistent current mode operation of high current DC superconducting magnet systems for applications in rotating machines, such as Magnetic Resonance Imaging (MRI) or fusion systems. The viability of the flux pump concept has been widely proven by laboratory experiments and research is now in progress for the design and optimization of flux pump devices for practical applications. It has been widely established that the dependence of the critical current density (J_c) on the temperature (T), the magnetic field magnitude (B), and the orientation (θ), has a substantial impact on the overall DC voltage obtained at the terminals, as well as on the current limit and the loss of the flux pump. Since HTS tapes produced by different manufacturers, they show different dependencies of J_c with the amplitude and the orientation of the magnetic field. They also give rise to different outputs when employed in flux pumps. In this paper, we evaluate and compare the performance of several commercial HTS tapes used for flux pumping purposes through numerical simulation. We also investigate the dependence of the flux pump 's performance on the operating temperatures. A 2D finite element numerical model is first developed and validated against experimental data at 77 K. Afterward, the same HTS dynamo apparatus used for validation is exploited for the comparison. The $J_c(B,\theta,T)$ and $n(B,\theta,T)$ relations, which characterize each different tape in the model, are reconstructed via artificial intelligence techniques based on the open-access database of the Robinson Research Institute. It is shown in the paper that certain tapes are more suitable than others for flux pump applications and that the best overall operating temperature is in the vicinity of 77 K.

Keywords: HTS dynamo machine; flux pump; finite element modeling; HTS tape

1. Introduction

Flux pumps represent a compact, contactless, and low-cost alternative to metal current leads and conventional power supplies for injecting and maintaining current in superconducting magnets [1–5]. In recent years, the flux pump's mechanism and charging capacity have been investigated both through numerical simulation [6–16] and through experimental tests [17–27]. Recent studies have also quantitatively addressed the potential advantages of the flux pumps in comparison to conventional solutions for the supply of superconducting magnets in practical applications. For the case of wind power generator exciters, Sung et al. calculated a heat load of 10.2 W using a flux pump against 31.8 W employing current leads when supplying a 12 MW wind generator [28,29], whilst the authors of this study had previously simulated the energetic performance of a dynamo designed for exciting the field winding of the EcoSwing wind turbine, reporting a potential 76% heat load reduction compared to the current leads based existing solution [30]. Rice et al. estimated a potential reduction of 90% and 98% in the cryogenic load for charging and maintaining 60 kA into the toroidal field coils of fusion magnets, proving to be a massive

space saver as well [31]. Flux pumps could also bring benefits to the biomedical industry, in fact, Wang et al. designed and constructed a compact 1.5 T HTS MRI system dedicated for human joint diagnosis [32,33], whilst Coombs et al. are constructing a portable MRI for human head scanning that employs a flux pump [34].

Despite the huge potential, the process of designing a flux pump with the desired performance is a non-trivial task due to its complex physical mechanism which ultimately results in intricate relationships between the flux pump specifications and the outputs. Therefore, recent studies have focused on the impact of the design parameters on the performance, including the FE frequency of rotation [35,36], the ratio between the permanent magnet and the HTS tape widths [37,38], the airgap [39,40], and the number of permanent magnets [41].

An effective design of flux pumps must rely on accurate modelling. The degradation of the critical current I_c of the HTS tapes due to the temperature T, as well as the magnetic field amplitude B and the orientation θ has been identified as a major factor that impacts the overall performance of the flux pump [42,43], both in terms of the output DC voltage and the efficiency. As the HTS tapes produced by different manufacturers have a different critical current behavior versus temperature and magnetic field, they perform differently when employed in flux pumps. In this paper, the performance of the flux pump based on different commercially available HTS tapes are numerically evaluated and compared to provide guidance on the selection of the best performing tape in the design of practical flux pump devices. The aim is to point out the main trends in the impact of the critical current density degradation on the flux pump outputs, as well as to provide a useful insight toward the future development of optimum-designed flux pumps. For each of the considered commercial tapes, the $I_c(B,θ,T)$ and $n(B,θ,T)$ curves available from the Robinson Research Institute "High-Temperature Superconductor critical current data" public database [43,44] have been used as input, and incorporated into the numerical model through artificial intelligence techniques. The consideration of the dependence of the critical current density J_c and the n exponent on the temperature T allowed for an investigation, for the first time, into the impact of T on the overall outputs and performance of the dynamo.

This paper is structured as follows. In Section 2, the finite element (FE) model that was developed for the numerical analysis is briefly resumed and validated over experimental results. The experimental flux pump apparatus reported in [21], employing a HTS tape with a 12 mm width produced by Superpower, is used to carry out the validation. In Section 3, the numerical model is used to simulate the performance of the same dynamo flux pump apparatus of [21] but employs different commercial HTS tapes. The performance results reported in this section include the *V-I* curves, as well as the output power, the loss, and the efficiency of the dynamos at different temperatures. This section also includes the results of the impact of the operating temperature on the outputs and performance. Finally, in Section 4, the main findings of this study are summarized in the conclusions.

2. Numerical Model and Validation against Experimental Results

2.1. The Volume Integral Elements Formulation (VIE) Model

The 2D numerical FE model that has been used to carry out this study is based on the Volume Integral Elements formulation (VIE) of the eddy current problem which is described in detail in [15]. The model solves an equivalent circuit of the HTS tape obtained by subdividing its cross section into a finite number of 2D elements along its width and by enforcing Equation (1) to be satisfied in the weak form over each element of the discretization.

$$\vec{E} = -\frac{\partial \vec{A}^{ext}}{\partial t} - \frac{\partial \vec{A}^{J}}{\partial t} - \nabla \phi \tag{1}$$

where ϕ is the electric scalar potential, the electromotive force is given by the sum of a contribution due to the time-varying field produced by the current induced in the super-conductor ($\partial \vec{A}^{J}/\partial t$ term) and a second contribution due to the varying external magnetic

field produced by the permanent magnet ($\partial \vec{A}^{ext}/\partial t$ term). Both the HTS and the two copper stabilizer layers are included in the numerical model, whereas the silver layer and the Hastelloy substrate are not considered due to their negligible effect. A constant resistivity of 0.19 $\mu\Omega$cm is assumed for the copper, whereas for the HTS layer, the electric field $\vec{E}$ is related to $\vec{J}$ by means of the *E-J* power law (2),

$$E = \frac{E_0}{J_C} \left| \frac{J}{J_C} \right|^{n-1} J \tag{2}$$

where E_0 is a conventional parameter used as a criterion for the definition of the conventional critical current density J_c (a value of 1 μV cm^{-1} is assumed), and the dimensionless n exponent is chosen to make (2) fit the experimental *E-J* line for a given tape. J_c and n depend on the temperature, as well as on the amplitude and orientation of the external magnetic field applied on the tape, hence, any commercial HTS tape is characterized by its specific $J_c(B,\theta,T)$ and $n(B,\theta,T)$ relations. These dependences are incorporated into the FE model by using artificial intelligence models [45], each of which is specific for one commercial HTS tape and is trained based on its own experimental $I_c(B,\theta,T)$ and $n(B,\theta,T)$ datasets taken from the Robinson Research Institute database [43,44].

The final system, written in Equation (3), is solved by enforcing the sum of all the currents flowing in the elements of the tape 2D discretization, which physically corresponds to imposing the transport current in the tape.

$$\bar{\bar{M}} \frac{d\bar{I}_w}{dt} = \bar{\bar{R}}\bar{I}_w + \bar{u} + \bar{1}V \tag{3}$$

where V is the resulting voltage at the terminals of the flux pump, $\bar{I}_w$ is the set of currents of the tape elements, $\bar{1}$ is a column vector of as many ones as the number of elements of the subdivision, $\bar{\bar{M}}$ is the self/mutual induction coefficients matrix of the elements, $\bar{\bar{R}}$ is the diagonal matrix of resistances, and $\bar{u}$ is the forcing terms due to the electromotive force caused by the external magnetic field of the permanent magnet.

2.2. Numerical Model Validation

The validation of the numerical model is carried out by simulating the flux pump apparatus of [21] and by comparing the numerical results with the experimental data. Figure 1a shows a 3D scheme of the dynamo flux pump tested in [21], whereas Figure 1b shows a 2D cross section of the dynamo and depicts the main parameters of the apparatus, that are also listed in Table 1. The flux pump of the experimental campaign employs a 12 mm wide HTS tape produced by Superpower, whose main characteristics are displayed in Table 2. An external electronic current supply is connected to the HTS tape of the flux pump to enforce the transport current I during the experiments, while voltage taps are used for measuring the voltage V of Figure 1a. This occurs when the flux pumping is taking place, that is when the HTS tape is cooled down to reach the superconducting state and the permanent magnet is rotating with angular velocity ω. Different rotation velocities, in the range 178.2–1489.8 rpm (corresponding to 2.97–24.83 Hz) are considered for the rotor in the experimental campaign. More details of the experimental set-up and its functioning can be found in [21]. The flux pump operation is simulated in current-driven conditions, which means that a constant transport current I is assigned in the FE model (for example, the case of open circuit corresponds to $I = 0$ A). The calculated DC voltage V of the flux pump (that is, the average voltage at the terminals in one period) is shown in Figure 2a for different values of the operating current and the frequency of the rotor. The corresponding experimental data are shown in Figure 2b. All the curves show a linear decrease of the DC terminal voltage with the operating current. The current I_{lim} at which the voltage becomes zero fix the limit of operability of the flux pump as a power supply. Beyond that value, the terminal voltage is reversed and so the power flows at the device terminal. Hence,

the electric power is absorbed rather than delivered to the flux pump terminals, and is converted, along with the mechanical power supplied to the rotor, in heat dissipation into the device. It can be noted that the model predicts lower values of both the DC voltage and the limit current for every frequency of rotation. In particular, the difference between the experimental DC open circuit voltage (at $I = 0$ A) and the numerical value is 32% on average, whereas the difference between the experimental and the numerical values of the limit current (at which $V = 0$ V) is 22% on average. The mismatch between the numerical and the experimental results Figure 2b, respectively, is mainly due to the uncertainty of the actual value of the airgap between the magnet and the tape during flux pump operation [8,39]. In fact, at least a 0.5 mm reduction of the airgap with respect to the measured value at room temperature is estimated to occur at 77 K in a similar flux pump apparatus due to thermal contractions [8]. Hence, in order to obtain a proper match between the model and the experimental *V-I* curves, a comparable reduction of the airgap needs to be considered. In Figure 2b the calculated *V-I* curves of the flux pump with a reduced airgap of 3 mm are shown. It can be observed that these curves fit the experimental data much better, with the error dropping to 3% and 6% for the DC open circuit voltages and the limit current of the flux pump, respectively. An applied airgap reduction of 0.7 mm with respect to the room temperature value needed for obtaining a proper fitting of the experimental data is in the range suggested in [8] due to thermal contraction. More accurate 3D models will be developed in future works to further improve the results in Figure 2b.


(**a**)　　　　　　　　　　　　　　　　　　　　(**b**)
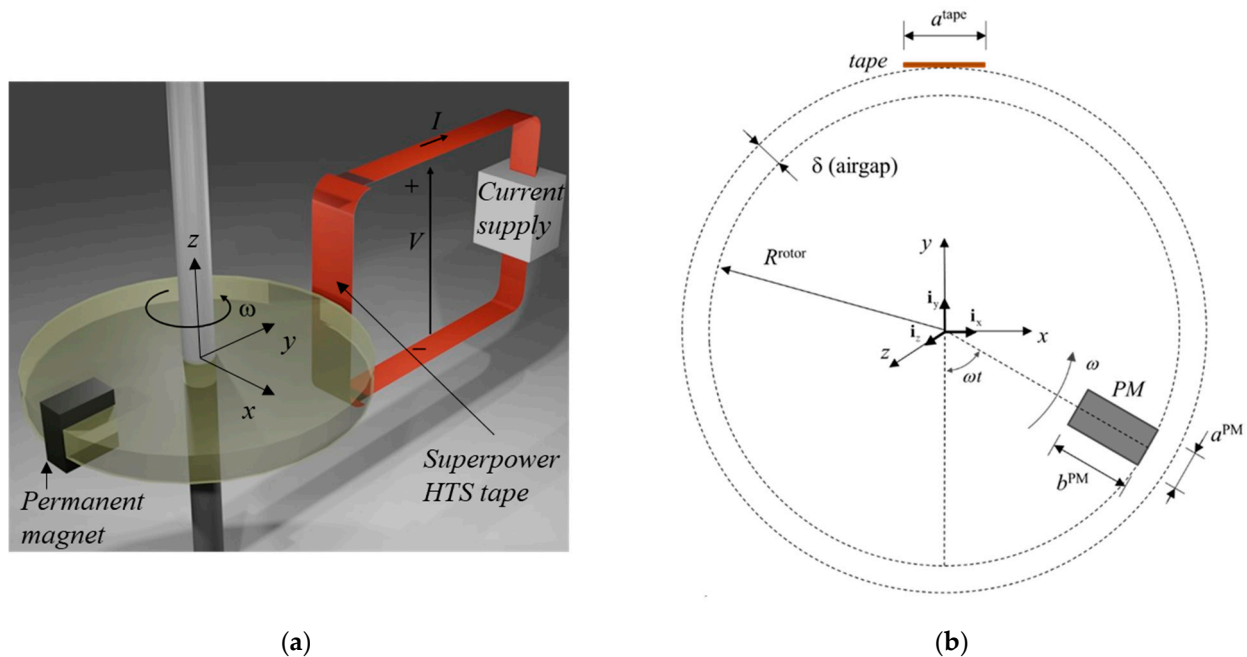
Figure 1. (**a**) Schematic illustration of the reference HTS dynamo flux pump used for simulation, and (**b**) schematic 2D section view of the flux pump (where *PM* stands for permanent magnet) [21].

Table 1. Main specifications of the reference HTS dynamo flux pump referred to Figure 1b.

Specification	Value
Width of the PM, a^{PM}	3.2 mm
Height of the PM, b^{PM}	12.7 mm
Depth of the PM, l^{PM}	12.7 mm
Remanence of the PM	1.3 T
Width of the HTS tape, a^{tape}	12 mm
Operating temperature	77 K
External radius of the rotor, R^{rotor}	35 mm
Airgap between the PM and the HTS tape, δ	3.7 mm

Table 2. Main characteristics of the Superpower HTS tape used in the reference HTS dynamo flux pump.

Specification	Value
Width of the HTS tape, a^{tape}	12 mm
Thickness of the HTS layer	1 μm
Thickness of the substrate (Hastelloy)	50 μm
Thickness of the Silver stabilizer layer	2 μm
Thickness of the Cu stabilizer layers (at the top and the bottom of the tape)	25 μm

(a)

(b)
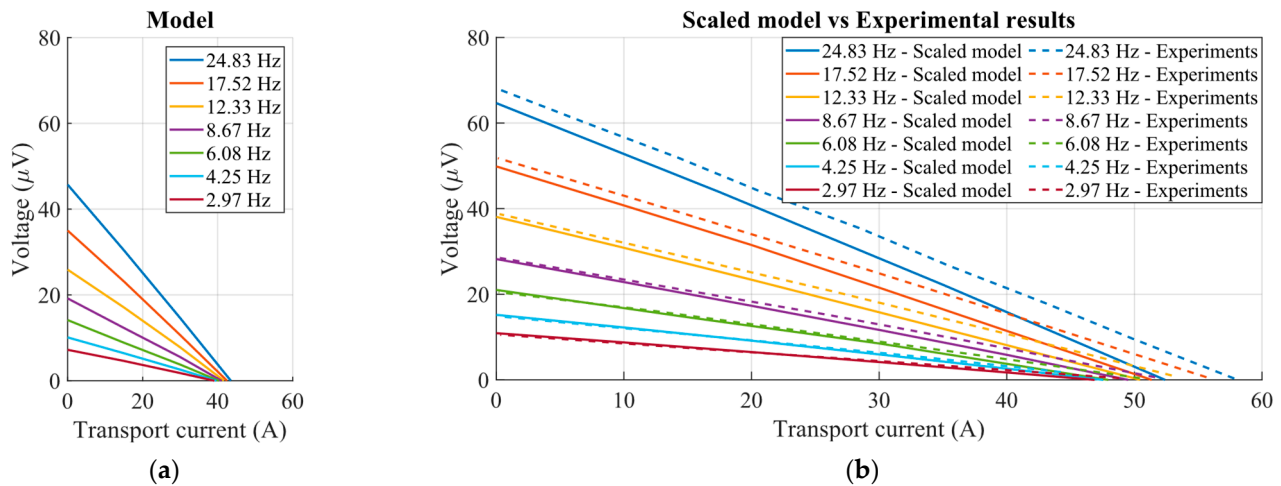
Figure 2. Numerical and experimental curves of the reference dynamo flux pump. The curves show the dependence of the DC terminal voltage on the transport current at different rotating frequencies; (**a**) numerical results obtained with the model using data from Table 1, comprising an airgap of 3.7 mm, (**b**) numerical results obtained with the scaled model using 3 mm air gap vs. experimental results from [21].

3. Results and Discussion-Performance of Different HTS Tapes for Flux Pump Applications

In this section, the performance of the dynamo flux pump in Table 1 (with a reduced airgap of 3.0 mm) employing different commercial HTS tapes and operating at 77.5 K are evaluated and compared, finding the best performer at this temperature. In applied superconductivity, 77.5 K is considered a relevant and strategic operating temperature in large-scale power applications, as it corresponds to the boiling temperature of nitrogen. The latter is then selected and the impact of temperature on the performance of the flux pump is investigated with reference to this HTS tape. For simplicity, all the quantitative performance indicators shown in this section refer to the basic flux pump design in Section 2, which employs one HTS tape and one rotating permanent magnet (PM) with an assigned layout and dimensions, and do not apply if optimized flux pump systems, with different layouts and/or dimensions, are considered. In comparative terms, however, the results of the present section apply to any flux pump device because a number of HTS tapes are periodically swept by a PM, similar to the case considered here. In particular, the selected tape with the best performance in terms of efficiency and DC output voltage for the considered basic flux pump design, will apply to other flux pump designs of practical interest.

3.1. Performance Comparison of Flux Pumps Based on Different Commercial HTS Tapes at 77.5 K

Using the corresponding data downloaded from [43], the following commercially available tapes have been simulated and compared.

- THEVA Pro-Line 2G HTS;
- Shanghai Superconductor Low Field High Temperature 2G HTS;
- SuperOx GdBCO 2G HTS;
- SuperOx YBCO 2G HTS;
- SuperPower Advanced Pinning 2G HTS;
- Fujikura FYSC 2G HTS;
- SuNAM HAN04200 2G HTS.

The main specifications in Table 1 are considered for all simulations, with exception to the airgap length, which, as discussed in Section 2, is set to 3 mm in order to reproduce the experimental data of the validation case with a good accuracy. A width of 12 mm is assumed for all the HTS tapes. The frequency of rotation of the permanent magnet is 24.83 Hz. An operating temperature of 77.5 K is considered for all simulated cases. The $I_c(B,\theta)$ and $n(B,\theta)$ curves at 77.5 K used for the simulations are taken from the Robinson Research Institute database [43,44]. The critical current characterization system that was used to acquire this data is fully described in [46]. The $I_c(B)$ per unit width at $\theta = 90°$ (field parallel to the tape) and the $I_c(\theta)$ per unit width curve at 0.3 T for all tapes are shown in Figure 3a,b as an example. Both the values shown are per unit width of tape. The $I_c(B)$ is limited to the interval 0–1 T as this is the desired range of field for flux pump applications. The results for all the tapes under the aforementioned operating conditions are reported in Figure 4. In particular, the dependence of the DC terminal voltage V on the operating current is shown. A wide spread of the open circuit voltage, ranging from 48 μV for the Fujikura tape to 93 μV for the SuperOx YBCO tape, can be observed from the figure. The limit of the current at which the flux pump can operate in the generator mode also depends on the tape. A limit current of 90 A is obtained for the THEVA tape, whereas a nearly double valued of 176 A is observed for the SuperOx YBCO tape. Despite having the lowest open circuit voltage, the Fujikura tape has the second largest limit current of the generator mode, which stresses the fact that the tape choice also affects the slope of the *V-I* curve and, hence, the deliverable power and efficiency. Figure 4b displays the AC losses of the dynamos at the different transport currents. It is stressed that the losses at a zero transport current, i.e., open circuit condition, is a non-zero and the trend of the AC losses against the transport current is quadratic, as previously observed in [15]. The power that is delivered by the dynamos and the corresponding efficiency are shown in Figure 4c,d, respectively. Because of the quasi-linear trend of the *V-I* curves, the maximum deliverable power and efficiency are closely located at half of the current limit of the generator mode. The maximum overall output power of 4.5 mW is reached by the SuperOx YBCO tape. This is not a surprise since it was already observed that this tape has both the largest open circuit voltage and the largest generator mode current limit. Since the losses are in the order of hundreds of mW whereas the output powers are in the order of the mW, low efficiencies in the range of 1% to 3.5% are reached. While low efficiencies are common in flux pumps, it is important to note that these results are notably low due to the small-scale laboratory apparatus employed in this study. Therefore, the efficiency range of 1–3.5% observed here holds no immediate practical significance. In the literature, efficiencies of up to 16% have been reported for dynamos [27], indicating substantial room for improvement.

Despite the fact that this paper highlights one of the main challenges of flux pumps, i.e., low efficiency, recent experimental studies reported more powerful dynamos, involving the largest number of permanent magnets and the largest rotating frequency, with a resulting efficiency of up to 16% [27], thus showing room for improvement for such technology.
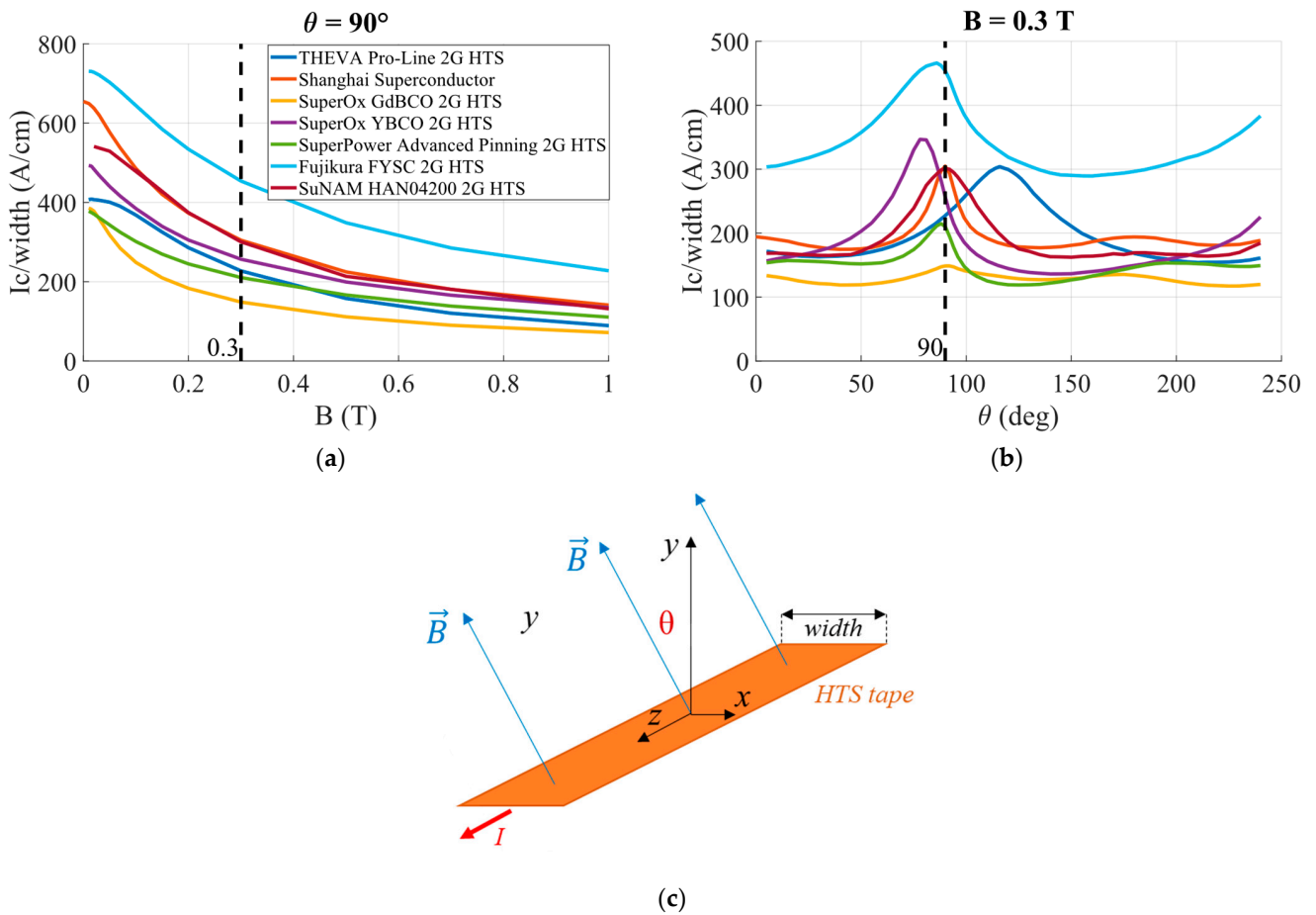
Figure 3. (**a**) I_c per unit width vs. B curve of the commercial HTS tapes at $T = 77.5$ K and θ = 90°
(field parallel to the tape), (**b**) I_c per unit width vs. θ curve of the commercial HTS tapes at $T = 77.5$ K
and B = 0.3 T, and (**c**) Schematic of the HTS tape and physical quantities in the experimental set-up
carried out to measure data in (**a**,**b**).
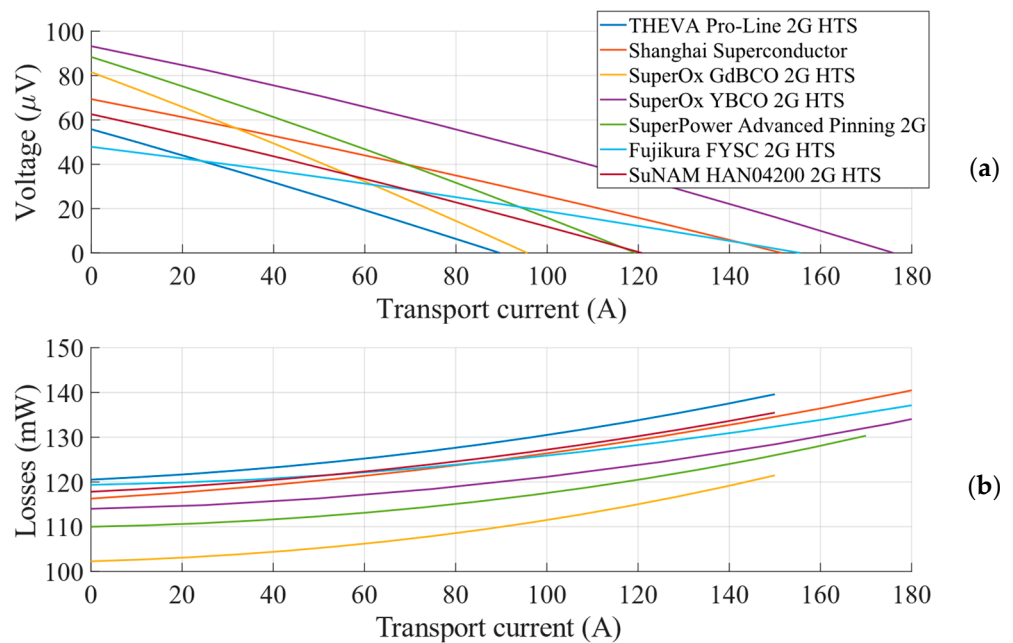
Figure 4. *Cont*.
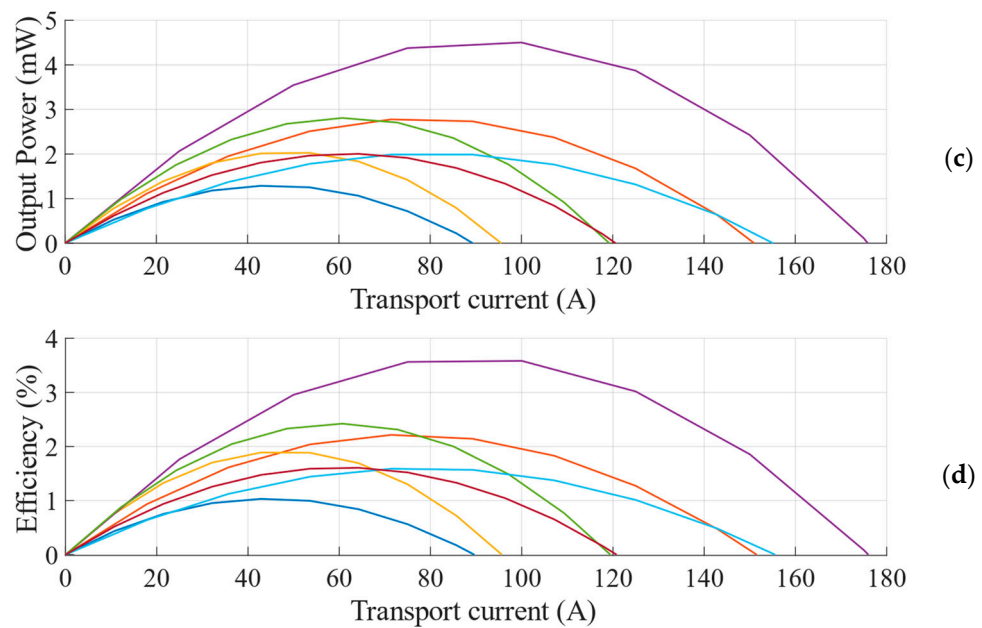
Figure 4. Performance and operating limits of the dynamo flux pumps employing different commercial HTS tapes at 77.5 K; (**a**) *V-I* curve, (**b**) loss of the dynamos at different transport currents, (**c**) Output power of the dynamos versus transport currents, and (**d**) efficiency of the dynamos versus transport currents.

3.2. Impact of Operating Temperature

Based on the results of Section 3.1, the SuperOx YBCO 2G HTS is chosen for carrying out the investigation of the impact of temperature on the performance of the dynamo flux pump. The following temperatures have been investigated: 55 K, 65 K, 70 K, 77.5 K, 80 K, and 85 K. Temperatures lower than 55 K have not been investigated due to the fact that the resulting performance of the flux pump in terms of open circuit voltage are too low to be of interest. At each operating temperature, the following performance and operating limits have been numerically evaluated:

- Open circuit voltage;
- Limit current of the generator mode;
- Maximum output power;
- AC loss in open circuit condition;
- Maximum efficiency.

The numerical results are reported in Figure 5. In particular, Figure 5a,b reports the dependence of the open circuit voltage and the limit current of the generator mode on the temperature. In these plots, it can be seen that the largest value of open circuit voltage is obtained between 80 K and 85 K (according to the polynomial interpolation), whereas the maximum value of the limit current is located at approximately 65 K, therefore it is not possible to find a temperature that maximizes both of these performances, and a trade-off is needed in the final design. It is worth noting that the open circuit voltage drastically drops for temperatures below about 75 K. This is explained by the improvement of the critical current of the tape and its reduced dependence on the external magnetic field which occurs at lower temperatures. In fact, the local non-linear resistivity is acknowledged to cause the voltage rectification in the flux pump [6], but the increase of the critical current and, most importantly, the reduced impact of the magnetic field at low temperatures makes the local resistivity drop. We also attribute the lower value of I_{lim} under 65 K to this. Indeed, at low temperatures the impact of the field produced by the permanent magnet is so minor that flux pumping barely happens, resulting in the *V-I* characteristic to escape the first quadrant and lay almost exclusively in the fourth one (low open circuit voltage and I_{lim}). On the other hand, the decrease of the open circuit voltage at high temperatures (above

80 K) is explained by the reduction of the non-linearity due to lower n values, whereas the decrease of the limit current is due to degradation of the superconducting properties which appears when the critical temperature is approached. Figure 5c,d shows how the energetic performance of the dynamo is affected by temperature.
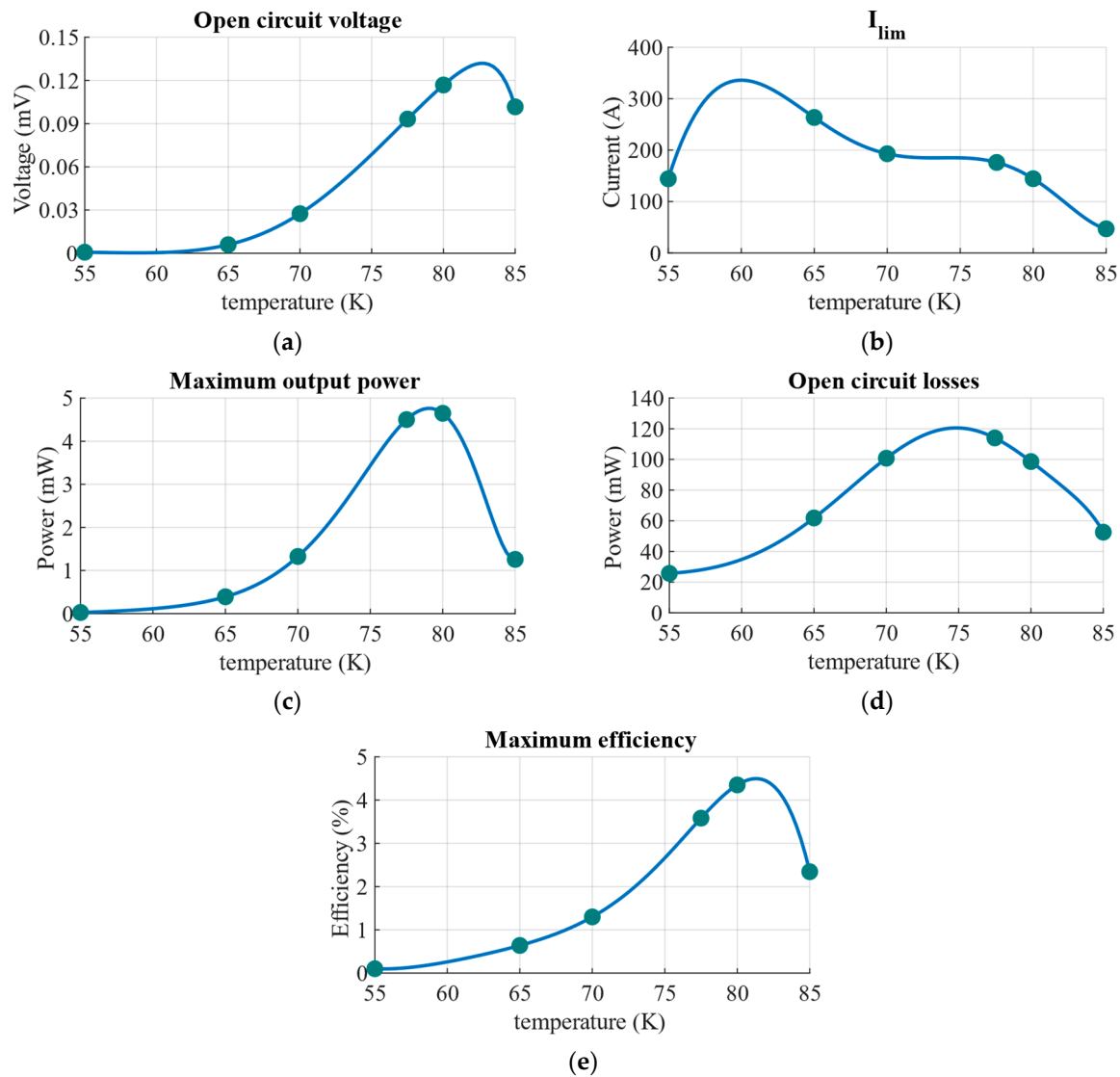
Figure 5. Impact of temperature on dynamo performance, the case of the SuperOx YBCO 2G HTS tape (points are the results of the model, lines are their polynomial interpolation): (**a**) Open circuit voltage vs. temperature, (**b**) I_{lim} vs. temperature, (**c**) Maximum output power vs. temperature, (**d**) Open circuit losses vs. temperature, and (**e**) Maximum efficiency vs. temperature.

In Figure 5c, the maximum output power that the dynamo can deliver to the load, which occurs approximately at half of the limit current of the generator mode, is maximized when the dynamo operates at roughly 80 K. In Figure 5d, it is observed that the largest value of open circuit AC loss lies between 70 K and 77.5 K. As a result, the maximum efficiency (over 4%) is clearly located around 80 K, as Figure 5e displays. Similar to Figure 4d, the low efficiency itself is not significant, as it pertains to a non-optimized laboratory-scale apparatus. However, what is crucial is its observed trend versus the transport current. It is plausible to assume that this same trend would scale towards higher efficiencies in the case of large-scale, optimized dynamos [27]. Based on the results of Figure 5, it could be discussed that choosing the operating temperature of a flux pump is no trivial task. Indeed, the generally poor efficiency should be a driver to make the flux pump operate at higher

temperatures, where both the efficiency and output power are maximized. However, it should not be forgotten that the very large current capability must be reached when the flux pump is needed for the supply of high current systems, like fusion magnets, and the best operating temperature in this regard is at about 65 K. Nevertheless, decreasing the operating temperature below 77.5 K is not viable due to the dramatic drop of the open circuit voltage that it involves. Therefore, the optimal temperature of the flux pump, allowing a maximum operating voltage, output power, and efficiency, is 77.5 K. An increased current capacity, when needed, must be reached by using more tapes in parallel. This choice is also technically convenient and cost-effective, as this temperature is obtained with a liquid nitrogen cooling at ambient pressure and does not require any additional apparatus.

4. Conclusions

In this paper, we evaluated and compared the performance and the operating limits in the generator mode of several commercial HTS tapes that can be considered for dynamo flux pumps. It is shown that the choice of the tape affects the voltage and current limits in the generator mode of almost up to 100%, whereas the maximum efficiency can be more than tripled (1% and 3.5% are obtained as the minimum and maximum best efficiency in this paper depending on the tapes used). These results stress the significant impact of the J_c(B,θ,T) and n(B,θ,T) dependence on the flux pump's performance. Furthermore, the impact of temperature on the open circuit voltage, the current limit in the generator mode, the maximum efficiency, the losses, and the maximum output power was assessed. The results showed that the best overall operating temperature of the flux pump is arguably in the vicinity of 77.5 K, if the goals are to optimize the output voltage and the efficiency, whereas the maximum current capacity occurs around 60 K, which also minimizes the losses. These are important and positive findings because they show that common cryogenic temperatures that can be reached with cheap liquid nitrogen are favorable for the effective operation of flux pumps. The numerical tool developed during this study and its results will be used for future research such as the design of large-scale flux pumps for a superconducting magnets power supply.

Author Contributions: Conceptualization, A.M.; Methodology, A.M. and G.R.; Software, G.R.; Validation, A.M. and G.R.; Formal analysis, A.M.; Investigation, G.R.; Resources, G.R.; Data curation, G.R.; Writing—original draft preparation, G.R.; Writing—review and editing, A.M.; Visualization, G.R.; Supervision, A.M.; Project administration, A.M. All authors have read and agreed to the published version of the manuscript.

Data Availability Statement: The original contributions presented in the study are included in the article material. Further inquiries can be directed to the corresponding author.

Conflicts of Interest: The authors declare no conflict of interest.

References

1. Van de Klundert, L.J.; ten Kate, H.H. Fully superconducting rectifiers and flux pumps part 1: Realized methods for flux pumping. *Cryogenics* **1981**, *21*, 195–206. [CrossRef]
2. Van de Klundert, L.J.M.; ten Kat, H.H.J. On fully superconducting rectifiers and fluxpumps. A review. Part 2: Commutation modes, characteristics and switches. *Cryogenics* **1981**, *21*, 267–277. [CrossRef]
3. Coombs, T.A. Superconducting flux pumps. *J. Appl. Phys.* **2019**, *125*, 230902. [CrossRef]
4. Coombs, T.A.; Geng, J.; Fu, L.; Matsuda, K. An overview of flux pumps for HTS coils. *IEEE Trans. Appl. Supercond.* **2017**, *27*, 1–6. [CrossRef]
5. Wen, Z.; Zhang, H.; Mueller, M. High Temperature Superconducting Flux Pumps for Contactless Energization. *Crystals* **2022**, *12*, 766. [CrossRef]

6. Mataira, R.C.; Ainslie, M.D.; Badcock, R.A.; Bumby, C.W. Origin of the DC output voltage from a high-Tc superconducting dynamo. *Appl. Phys. Lett.* **2019**, *114*, 162601. [CrossRef]
7. Ghabeli, A.; Ainslie, M.; Pardo, E.; Quéval, L.; Mataira, R. Modeling the charging process of a coil by an HTS dynamo-type flux pump. *Supercond. Sci. Technol.* **2021**, *34*, 84002. [CrossRef]
8. Ghabeli, A.; Pardo, E.; Kapolka, M. 3D modeling of a superconducting dynamo-type flux pump. *Sci. Rep.* **2021**, *11*, 10296. [CrossRef]
9. Ainslie, M.; Queval, L.; Mataira, R.; Badcock, R.; Bumby, C. Modelling an HTS Dynamo Using a Segregated Finite-Element Model. 2019. Available online: https://core.ac.uk/download/pdf/237398489.pdf (accessed on 13 September 2023).
10. Ainslie, M.; Grilli, F.; Quéval, L.; Pardo, E.; Perez-Mendez, F.; Mataira, R.; Morandi, A.; Ghabeli, A.; Bumby, C.; Brambilla, R. A new benchmark problem for electromagnetic modelling of superconductors: The high-Tc superconducting dynamo. *Supercond. Sci. Technol.* **2020**, *30*, 105009. [CrossRef]
11. Prigozhin, L.; Sokolovsky, V. Two-dimensional model of a high-Tc superconducting dynamo. *IEEE Trans. Appl. Supercond.* **2021**, *31*, 5201107. [CrossRef]
12. Prigozhin, L.; Sokolovsky, V. Fast solution of the superconducting dynamo benchmark problem. *Supercond. Sci. Technol.* **2021**, *34*, 65006. [CrossRef]
13. Campbell, A.M. A finite element calculation of flux pumping. *Supercond. Sci. Technol.* **2017**, *30*, 125015. [CrossRef]
14. Wen, Z.; Zhang, H.; Mueller, M. Sensitivity analysis and machine learning modelling for the output characteristics of rotary HTS flux pumps. *Supercond. Sci. Technol.* **2021**, *34*, 125019. [CrossRef]
15. Morandi, A.; Russo, G.; Fabbri, M.; Soldati, L. Energy balance, efficiency and operational limits of the dynamo type flux pump. *Supercond. Sci. Technol.* **2022**, *35*, 65011. [CrossRef]
16. Ainslie, M.D. Numerical modelling of high-temperature superconducting dynamos: A review. *Superconductivity* **2022**, *5*, 100033. [CrossRef]
17. Hoffmann, C.; Pooke, D.; Caplin, A.D. Flux Pump for HTS Magnets. *IEEE Trans. Appl. Supercond.* **2011**, *21*, 1628–1631. [CrossRef]
18. Bumby, C.W.; Pantoja, A.E.; Sung, H.J.; Jiang, Z.; Kulkarni, R.; Badcock, R.A. Through-Wall Excitation of a Magnet Coil by an External-Rotor HTS Flux Pump. *IEEE Trans. Appl. Supercond.* **2016**, *26*, 500505. [CrossRef]
19. Fu, L.; Matsuda, K.; Lecrevisse, T.; Iwasa, Y.; Coombs, T. A flux pumping method applied to the magnetization of YBCO superconducting coils: Frequency, amplitude and waveform characteristics. *Supercond. Sci. Technol.* **2016**, *29*, 4LT01. [CrossRef]
20. Zhang, Y.; Wang, W.; Ye, H.; Wang, X.; Gao, Y.; Zhou, Q.; Liu, X.; Lei, Y. Compact Linear-Motor Type Flux Pumps with Different Wavelengths for High-Temperature Superconducting Magnets. *IEEE Trans. Appl. Supercond.* **2020**, *30*, 5000305. [CrossRef]
21. Mataira, R.; Ainslie, M.; Pantoja, A.; Badcock, R.; Bumby, C. Mechanism of the high-Tc superconducting dynamo: Models andexperiment. *Phys. Rev. Appl.* **2020**, *14*, 24012. [CrossRef]
22. Fu, L.; Matsuda, K.; Shen, B.; Coombs, T. HTS flux pump charging an HTS coil: Experiment and modeling. *IEEE Trans. Appl. Supercond.* **2021**, *31*, 1–5. [CrossRef]
23. Geng, J.; Bumby, C.W.; Badcock, R.A. Maximising the current output from a self-switching kA-class rectifier flux pump. *Supercond. Sci. Technol.* **2020**, *33*, 45005. [CrossRef]
24. Gawith, J.D.D.; Geng, J.; Li, C.; Shen, B.; Zhang, X.; Ma, J.; Coombs, T.A. A half-bridge HTS transformer–rectifier flux pump withtwo AC field-controlled switches. *Supercond. Sci. Technol.* **2018**, *31*, 85002. [CrossRef]
25. Ma, J.; Geng, J.; Gawith, J.; Zhang, H.; Li, C.; Shen, B.; Dong, Q.; Yang, J.; Chen, J.; Li, Z.; et al. Rotating permanent magnets based flux pump for HTS no-insulation coil. *IEEE Trans. Appl. Supercond.* **2019**, *29*, 1–6. [CrossRef]
26. Hamilton, K.; Pantoja, A.E.; Storey, J.G.; Jiang, Z.; Badcock, R.A.; Bumby, C.W. Design and performance of a "squirrel-cage" dynamo-type HTS flux pump. *IEEE Trans. Appl. Supercond.* **2018**, *28*, 1–5. [CrossRef]
27. Hamilton, K.; Mataira, R.; Geng, J.; Bumby, C.; Carnegie, D.; Badcock, R. Practical estimation of HTS dynamo losses. *IEEE Trans. Appl. Supercond.* **2020**, *30*, 4703105. [CrossRef]
28. Sung, H.J.; Badcock, R.A.; Jiang, Z.; Choi, J.; Park, M.; Yu, I.K. Design and Heat Load Analysis of a 12 MW HTS Wind Power Generator Module Employing a Brushless HTS Exciter. *IEEE Trans. Appl. Supercond.* **2016**, *26*, 5205404. [CrossRef]
29. Tuvdensuren, O.; Sung, H.J.; Go, B.S.; Le, T.T.; Park, M.; Yu, I.K. Structural design and heat load analysis of a flux pump-based HTS module coil for a large-scale wind power generator. *J. Phys. Conf. Ser. IOP Publ.* **2018**, *1054*, 12084. [CrossRef]
30. Russo, G.; Morandi, A. A Numerical Study on the Energization of the Field Coils of a Full-Size Wind Turbine with Different Types of Flux Pumps. *Energies* **2022**, *15*, 5392. [CrossRef]
31. Rice, J.H.P.; Geng, J.; Bumby, C.W.; Weijers, H.W.; Wray, S.; Zhang, H.; Schoofs, F.; Badcock, R.A. Design of a 60 kA Flux Pump for Fusion Toroidal Field Coils. *IEEE Trans. Appl. Supercond.* **2022**, *32*, 5500205. [CrossRef]
32. Wang, X.; Wang, W.; Gao, Y.; Lei, Y.; Ye, H.; Zhang, Y.; Zhou, Q.; Zhu, Y.; Liu, X. An HTS NI Magnet Charged by Multiple Flux Pumps: Construction and Test of the Prototype. *IEEE Trans. Appl. Supercond.* **2020**, *30*, 4602005. [CrossRef]
33. Wei, J.; Wang, W.; Zhou, L.; Zhang, C.; Wang, X.; Yang, Z.; Xiong, C.; Yang, C.; Long, R.; Wu, C.; et al. Improving the central magnetic field of an HTS magnet using multiple flux pumps. *IEEE Trans. Appl. Supercond.* **2022**, *32*, 4602705. [CrossRef]
34. Öztürk, Y.; Shen, B.; Williams, R.; Gawith, J.; Yang, J.; Ma, J.; Carpenter, A.; Coombs, T. Current Status in Building a Compact and Mobile HTS MRI Instrument. *IEEE Trans. Appl. Supercond.* **2021**, *31*, 1–5. [CrossRef]
35. Ainslie, M.D.; Quéval, L.; Mataira, R.C.; Bumby, C.W. Modelling the frequency dependence of the open-circuit voltage of a high-T c superconducting dynamo. *IEEE Trans. Appl. Supercond.* **2021**, *31*, 4900407. [CrossRef]

36. Bumby, C.W.; Phang, S.; Pantoja, A.E.; Jiang, Z.; Storey, J.G.; Sung, H.-J.; Park, M.; Badcock, R.A. Frequency dependent behavior of a dynamo-type HTS flux pump. *IEEE Trans. Appl. Supercond.* **2016**, *27*, 1–5. [CrossRef]

37. Mataira, R.; Ainslie, M.D.; Badcock, R.; Bumby, C.W. Modeling of Stator Versus Magnet Width Effects in High-T$_c$ Superconducting Dynamos. *IEEE Trans. Appl. Supercond.* **2020**, *30*, 1–6. [CrossRef]

38. Pantoja, A.E.; Jiang, Z.; Badcock, R.A.; Bumby, C.W. Impact of stator wire width on output of a dynamo-type HTS flux pump. *IEEE Trans. Appl. Supercond.* **2016**, *26*, 4805208. [CrossRef]

39. Ghabeli, A.; Pardo, E. Modeling of airgap influence on DC voltage generation in a dynamo-type flux pump. *Supercond. Sci. Technol.* **2020**, *33*, 35008. [CrossRef]

40. Jiang, Z.; Bumby, C.W.; Badcock, R.A.; Sung, H.J.; Long, N.J.; Amemiya, N. Impact of flux gap upon dynamic resistance of a rotating HTS flux pump. *Supercond. Sci. Technol.* **2015**, *28*, 115008. [CrossRef]

41. Zhou, P.; Ren, G.; Ainsile, M.; Ghabeli, A.; Zhang, S.; Zhai, Y.; Ma, G. Impact of Magnet Number on the DC Output of a Dynamo-Type HTS Flux Pump. *IEEE Trans. Appl. Supercond.* **2023**, *33*, 4603509. [CrossRef]

42. Geng, J.; Matsuda, K.; Fu, L.; Fagnard, J.-F.; Zhang, H.; Zhang, X.; Shen, B.; Dong, Q.; Baghdadi, M.; A Coombs, T. Origin of dc voltage in type II superconducting flux pumps: Field, field rate of change, and current density dependence of resistivity. *Phys. D Appl. Phys.* **2016**, *49*, 11LT01. [CrossRef]

43. Robinson Research Institute. Available online: http://htsdb.wimbush.eu/ (accessed on 13 September 2023).

44. Wimbush, S.C.; Strickland, N.M. A Public Database of High-Temperature Superconductor Critical Current Data. *IEEE Trans. Appl. Supercond.* **2017**, *27*, 1–5. [CrossRef]

45. Russo, G.; Yazdani-Asrami, M.; Scheda, R.; Morandi, A.; Diciotti, S. Artificial intelligence-based models for reconstructing the critical current and index-value surfaces of HTS tapes. *Supercond. Sci. Technol.* **2022**, *35*, 124002. [CrossRef]

46. Strickland, N.M.; Hoffmann, C.; Wimbush, S.C. A 1 kA-class cryogen-free critical current characterization system for superconducting coated conductors. *Rev. Sci. Instrum.* **2014**, *85*, 113907. [CrossRef]